Progress In Electromagnetics Research B, Vol. 37, 205–235, 2012

DERIVATION OF HOMOGENEOUS PERMITTIVITY OF COMPOSITE MATERIALS WITH ALIGNED CYLINDRICAL INCLUSIONS FOR CAUSAL ELECTROMAGNETIC SIMULATIONS

F. de Paulis[1,*], M. H. Nisanci[1], M. Y. Koledintseva[2], J. L. Drewniak[2], and A. Orlandi[1]

[1]UAq EMC Laboratory, University of L'Aquila, L'Aquila, Italy

[2]Missouri S&T EMC Laboratory, Missouri University of Science and Technology, Rolla, MO, USA

Abstract—The paper gives an analytical transition from the Maxwell Garnett model of a biphasic mixture (dielectric host and dielectric or conducting inclusions) to the parameters of a single- or double-term Debye representation of the material frequency response. The paper is focused on modeling biphasic mixtures containing cylindrical inclusions. This is practically important for engineering electromagnetic absorbing composite materials, for example, containing carbon fibers. The causal Debye representation is important for incorporation of a composite material in numerical electromagnetic codes, especially time-domain techniques, such as the finite-difference time-domain (FDTD) technique. The equations derived in this paper are different for different types of host and inclusion materials. The corresponding cases for the typical combinations of host and inclusion materials are considered, and examples are provided. The difference between the original Maxwell Garnett model and the derived Debye model is quantified for validating the proposed analytical derivation. It is demonstrated that in some cases the derived equivalent Debye model well approximates the frequency characteristics of the homogeneous model based on the MGA, and in some cases there is an exact match between Debye and Maxwell Garnett models.

Received 28 July 2011, Accepted 27 October 2011, Scheduled 21 December 2011

* Corresponding author: Francesco De Paulis (francesco.depaulis@univaq.it).

1. INTRODUCTION

Composite materials are largely employed due to their outstanding mechanical and electrical properties, and they are widespread in many civil and military applications, e.g., microwave filters, printed circuit boards, electromagnetic shields, and radar radomes [1, 2]. These materials allow for high design flexibility, since they can be adapted to achieve complex shapes and ad-hoc strength levels, provide sound and heat isolations, as well as good electromagnetic shielding protection [3–7]. Micro/nano fabrication processes, indeed, allow for making composites of carbon nanotubes, which could be used in various devices, e.g., actuators [8–12]. In the early application design stages, the knowledge of the effective electromagnetic properties of composite materials is essential for a quick and appropriate layout, based on numerical electromagnetic simulations.

In the present-day literature, there is a variety of different homogenization mixing rules, applicable to biphasic mixtures to retrieve their effective dielectric properties, e.g., Bruggeman [13], McLachlan et al. [14], and Maxwell Garnett models [15]. These theories describe the frequency-dependent properties of homogenized composites depending on mechanical and electrical properties of host and inclusions, such as inclusion shape, volume fraction, electrical conductivity, and permittivity. These models have different degree of accuracy and ranges of validity [16].

The Maxwell Garnett approximation (MGA) [15] is a quasi-static model for electromagnetic properties of mixtures with comparatively small inclusions embedded inside a host material [17]. The assumptions for applying the MGA are linearity of a biphasic material (neither the host, nor the inclusion behavior depends on the intensity of the applied electromagnetic field); inclusion size is smaller than the wavelength in the effective medium; and concentration of inclusion is below the percolation threshold, if inclusions are conductive. If the inclusions are spheres with a random distribution, the highest volume fraction of inclusions should be below approximately 30% [18]. The concept of percolation threshold is applicable only if there are conducting particles in the composite. If the mixture is dielectric-dielectric, the concept of the percolation is irrelevant. When conductive inclusions are considered, in general, the percolation threshold depends on many factors, including particle distribution and orientation, shape of inclusion (aspect ratio), physical properties of a polymer matrix, inclusion-matrix interactions, leading to an ability of inclusions to build chains within the matrix. If inclusions are considered to be aligned, as in this work, the assumption of uniform distribution in space, and

also the non overlapping condition is assumed; therefore, ideally, the percolation condition is always avoided leading to the possibility to neglect the percolation threshold, and thus any limitation on the volume fraction [19–25].

The MGA may be applied to different types of ellipsoidal inclusions, including spherical and cylindrical particles, which may be either randomly distributed, or arranged as a regular lattice. [25–31]. An electromagnetically isotropic equivalent homogeneous material can be obtained based on the electrical and geometrical properties of a composite with randomly dispersed inclusions. If inclusions are regularly distributed and aligned, instead, the resultant homogeneous medium is anisotropic, and its electromagnetic parameters such as the electric permittivity should be described by a tensor [17].

The application of the MGA leads to an equivalent homogeneous medium described by a complex frequency dependent dielectric permittivity $\varepsilon_{eff\text{-}MG}(f)$. If intrinsic electromagnetic parameters of ingredients of a composite satisfy causality, the effective parameters, calculated using the MGA, should also be causal. If the effective permittivity $\varepsilon_{eff\text{-}MG}(f)$ is represented in the Debye form, then the causality expressed through the Kramers-Krönig relations (KKR) [32–34] is satisfied automatically. This is important for simulation convergence of numerical codes in time domain, if the material with $\varepsilon_{eff\text{-}MG}(f)$ is modeled using one of the time-domain numerical electromagnetic technique [35]. Numerical simulations in frequency domain, e.g., the ones employing the finite-element method or the method of moments, may simply neglect the KKR, and it will not affect convergence, though computational results may be unphysical. However, violation of the KKR leads to the divergence of simulations in time domain. Appendix A contains an analytical proof that the real and imaginary parts of permittivity in the first-order Debye model are related as the KKR.

The purpose of this study is to analytically obtain the parameters of the one-term or two-term Debye model from the geometry-based MGA for effective permittivity of a mixture containing dielectric and/or conductive aligned cylindrical inclusions. The total or approximate equivalence between the two models (Maxwell Garnett and Debye) allows for simple incorporation of the MGA into time-domain electromagnetic simulations. The complete analytical derivation of the Debye model parameters from the intrinsic material parameters of the composite phases, e.g., their geometry and volume fraction is presented below in this paper.

Several cases of different combinations of electrical properties of host and inclusion materials will be considered in this paper. The host

material may be with either constant, or Debye frequency-dependent permittivity, and the inclusions may be made of a lossy dielectric, or a conductive material. The corresponding analytical relations for the Debye parameters from the MGA will be derived. Some examples will be presented for validating the proposed approach by comparing the original MGA and the computed Debye model.

2. DESCRIPTION OF THE ANALYTICAL PROCEDURE

The MGA model can be used to calculate the frequency-dependent effective permittivity of composite structures with aligned cylindrical inclusions from their geometrical parameters [15, 36, 37]. The present study deals with aligned inclusions. For this reason, the composite is anisotropic. Hence two values of the effective dielectric permittivity should be considered: one along the inclusion axes, i.e., z-axis, and one for the directions normal to the inclusion axes, i.e., in the (xy) plane [17, 37]. The assumption is that there is no cross-coupling among different directions, thus describing the anisotropic mixture by a diagonal tensor,

$$\overleftrightarrow{\varepsilon}_{\textit{eff-MG}}(\omega) = \begin{bmatrix} \varepsilon_{\textit{eff-MG},x}(\omega) & 0 & 0 \\ 0 & \varepsilon_{\textit{eff-MG},y}(\omega) & 0 \\ 0 & 0 & \varepsilon_{\textit{eff-MG},z}(\omega) \end{bmatrix}, \quad \text{(1a)}$$

where each component, $\varepsilon_{\textit{eff-MG},\alpha} = \varepsilon_{\infty,\alpha} + \chi_\alpha(\omega)$, is calculated as in (1b). The notation in (1a) includes explicitly the frequency dependence of the permittivity values associated to the Maxwell Garnett mixing rule; it is omitted in the following equations for simplicity. The derivation of (1b) is detailed in [38], where the cylindrical inclusions are assumed to be ellipsoidal scatterers. The effective permittivity of the medium in each direction is derived starting from the relation between the electric field inside and outside the scatterers, and the induced dipole moment due to an exciting field.

$$\varepsilon_{\textit{eff-MG},x,y,z} = \varepsilon_e + f\varepsilon_e \frac{\varepsilon_i - \varepsilon_e}{\varepsilon_e + (1-f)N_{x,y,z}(\varepsilon_i - \varepsilon_e)}. \quad \text{(1b)}$$

In (1b), the parameters ε_e and ε_i are the host and inclusion relative permittivity values, respectively, and f is the volume percentage (volume fraction) of the inclusions. The same Eq. (1b) applies to all three permittivity values, since they depend on the polarization factor N_k of elongated cylindrical inclusions [39, 40], assuming that the axes of the cylindrical inclusions are aligned in the z-direction. The depolarization factors given in (2) are evaluated from the equation

given in [38, 41]. The closed form expression in (2b) can be obtained if the ellipsoids are of the shape of elongated prolate spheroids.

$$N_x = N_y = \frac{1 - N_z}{2}, \tag{2a}$$

$$N_z = \frac{1}{2} \frac{\ln\left(\frac{a+\sqrt{a^2-1}}{a-\sqrt{a^2-1}}\right) a - 2\sqrt{a^2-1}}{\left(\sqrt{a^2-1}\right)^3}. \tag{2b}$$

where $a = l/d$ is the aspect ratio of the inclusions, defined as the ratio between cylinder length (l) and inclusion diameter (d). The resulting N_z is in inverse proportion to the aspect ratio a, thus it assumes very small values for large aspect ratios, being consistent to the case limit of infinite thin ellipsoids, having one axes much larger than the other two. In this case limit the depolarization factor is 0 along the main axes, i.e., z-direction, and 0.5 along the other two directions, i.e., x and y directions. The calculation of N_x and N_y in (2a) is obtained taking into account the relationship that link the three depolarization factors, $N_x + N_y + N_z = 1$, as demonstrated in [41].

In this study, based on the practical cases of materials behavior at microwaves, the host material permittivity ε_e in (1b) is considered to be constant, or having a first order Debye frequency dependence,

$$\varepsilon_{Dx,y,z} = \varepsilon_\infty + \frac{(\varepsilon_s - \varepsilon_\infty)}{1 + j\omega\tau}, \tag{3a}$$

and inclusions are assumed to be made of a lossy dielectric, characterized by the frequency dependent permittivity as in (3a), or a conductive material, whose complex permittivity is characterized by (3b).

$$\varepsilon_{Dx,y,z} = \varepsilon_\infty + \frac{\sigma}{j\omega\varepsilon_0}, \tag{3b}$$

In (3a) and (3b), ε_s is the static dielectric constant and ε_∞ is the high frequency ("optic limit") relative permittivity, τ is the relaxation time, σ is the conductivity (of the inclusion material), ω is the angular frequency, and $\varepsilon_0 = 8.85.10^{-12}$ F/m is the permittivity of free space.

Various optimization procedures, e.g., a genetic algorithm [42–44], or a curve-fitting based on the non-linear regression analysis [45], are typically employed in order to extract the frequency dependent Debye model based on composite geometrical parameters. However, in general, these procedures are not very efficient, since they are time- and memory-consuming, need special skills to work with those optimization procedures, and sometimes accuracy of the fit depends on the initial guess for the search pool parameters. An analytical derivation of the

Debye model from the equivalent permittivity obtained applying the MG model is more attractive.

According to the procedures described in [36, 46–49], there is not perfect equivalence between the Debye and the MGA models, thus a rigorous analytical relation cannot be found. An alternative could be considered by looking at the trends of the real and imaginary parts of $\varepsilon_{eff\text{-}MG}$ representing one of the components of the tensor in (1) An example of the Debye-like $\varepsilon_{eff\text{-}MG}$ is shown in Figure 1 for inclusions made of Barium Titanate ($BaTiO_3$ with Debye dispersive parameters $\varepsilon_{is} = 1900$, $\varepsilon_{i\infty} = 280$, $\tau_i = 2 \cdot 10^{-9}$) in a host material with constant permittivity $\varepsilon_e = 2.2$. The idea is to analytically derive the static permittivity ε_{sD} as the limit for $\omega \to 0$ of $\mathrm{Re}(\varepsilon_{eff\text{-}MG})$, and $\varepsilon_{\infty D}$ for $\omega \to \infty$ of $\mathrm{Im}(\varepsilon_{eff\text{-}MG})$ [39], as can be seen in qualitatively shown in Figure 1(a).

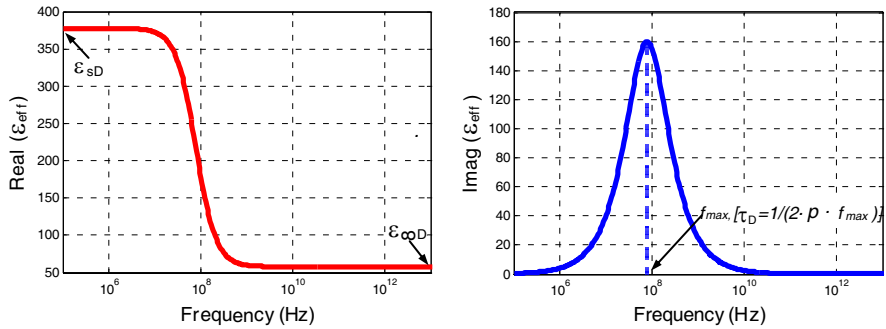

Figure 1. $\varepsilon_{eff\text{-}MG}$ for $a = 500$, $f = 20.1$, $\varepsilon_e = 2.2$ and $\varepsilon_i = BaTiO_3$. (a) Real part. (b) Imaginary part.

More precisely the static and optic limit permittivity values should be derived for the three terms in (1a), $\varepsilon_{sDx,y,z}$ and $\varepsilon_{\infty Dx,y,z}$, respectively,

$$\varepsilon_{sDx,y,z} = \lim_{\omega \to 0} \mathrm{Re}\left(\varepsilon_{eff-MGx,y,z}\right) \tag{4a}$$

$$\varepsilon_{\infty Dx,y,z} = \lim_{\omega \to \infty} \mathrm{Re}\left(\varepsilon_{eff-MGx,y,z}\right) \tag{4b}$$

After getting the $\varepsilon_{sDx,y,z}$ and $\varepsilon_{\infty Dx,y,z}$, the last term to be evaluated is the relaxation time $\tau_{Dx,y,z}$; the MG model in (1) is set equal to the general form of the equivalent Debye model in (3a), as in

$$\varepsilon_{eff-MGx,y,z} = \varepsilon_{\infty Dx,y,z} + \frac{\left(\varepsilon_{sDx,y,z} - \varepsilon_{\infty Dx,y,z}\right)}{1 + j\omega\tau_{Dx,y,z}}. \tag{5}$$

Equation (5) is then solved for $\tau_{Dx,y,z}$ as

$$\tau_{Dx,y,z}(\omega) = \frac{\dfrac{\varepsilon_{sDx,y,z} - \varepsilon_{\infty Dx,y,z}}{\varepsilon_{eff-MGx,y,z} - \varepsilon_{\infty Dx,y,z}} - 1}{j\omega}. \tag{6}$$

As stated before, the MGA applied to aligned cylindrical inclusions cannot be described perfectly in terms of a Debye model. Therefore, (6) provides not a single real value, but a complex and frequency-dependent relaxation time. However, the imaginary part has been found to be much smaller than the real part for all the cases investigated ($\mathrm{Im}[\tau_{Dx,y,z}(\omega)] \approx 10^{-6} \cdot \mathrm{Re}[\tau_{Dx,y,z}(\omega)]$), and it can be simply neglected. Furthermore, the real part looks like a step function with the higher value at the lower frequencies close to d.c., and the lower value for $\omega \to \infty$. Although the variation in the real part is very small ($\mathrm{Re}[\tau_{Dx,y,z}(\omega = 0)] \approx \mathrm{Re}[\tau_{Dx,y,z}(\omega \to \infty)]$), the step occurs at frequencies ($\approx 10^{15}$–10^{20} Hz) much beyond than the validity of the MGA formulation. Therefore, the relaxation time of the equivalent Debye model can be expressed as the d.c. limit of the real part of (6) as

$$\tau_{Dx,y,z} = \lim_{\omega \to 0} \mathrm{Re}(\tau_{Dx,y,z}(\omega)) = \lim_{\omega \to 0} \mathrm{Re}\left(\frac{\dfrac{\varepsilon_{sDx,y,z} - \varepsilon_{\infty Dx,y,z}}{\varepsilon_{eff-MGx,y,z} - \varepsilon_{\infty Dx,y,z}} - 1}{j\omega} \right). \tag{7}$$

The set of Eqs. (4)–(7) allows for a complete derivation of the Debye parameters. These equations can be specified for the most practical (in microwave applications) combinations of host and inclusion type of materials, such as constant and Debye-like permittivity host, and lossy dielectric (Debye-like) and conductive

Table 1. Case overview.

		Host ε_e			Inclusion ε_i			
		ε_{es}	$\varepsilon_{e\infty}$	τ_e	ε_{is}	$\varepsilon_{i\infty}$	τ_i	σ_i
Case 2	A		2.2		1900	280	$2 \cdot 10^{-9}$	
Case 3	A	2.5	2.2	$8 \cdot 10^{-12}$		280		
Case 4	A	2.5	2.2	$8 \cdot 10^{-12}$	1900	280	$2 \cdot 10^{-9}$	
Case 5	A		2.2			2		$4 \cdot 10^{3}$
	B		2.2			2		$4 \cdot 10^{4}$
Case 6	A	2.5	2.2	$8 \cdot 10^{-12}$		2		$4 \cdot 10^{3}$
	B	2.5	2.2	$8 \cdot 10^{-12}$		2		$4 \cdot 10^{4}$

inclusion material. Thus the three parameter of the equivalent Debye model, $\varepsilon_{eff-Dx,y,z}$, can be expressed in terms of the specific electrical and geometrical properties of the host and inclusions ε_e, ε_i, f and a values. A specific set of equations are derived for the five different cases listed in Table 1.

The values given in Table 1 are mainly associated with the commercial composite materials, widely used for shielding and other microwave applications. The Teflon (PTFE) material is usually employed as the base material (host matrix) for design of shields for microwave frequencies (100 MHz–10 GHz). This material [50] is almost non-dispersive in the frequency range of interest, and its loss factor can be neglected, thus the constant value $\varepsilon_s = 2.2$ is employed [51]. Inclusions in the Cases 2 and 4 are made of Barium Titanate ($BaTiO_3$) [52]. The latter provides good insulation properties and high dielectric contrast with the host matrix. As for the conducting inclusions, the conductivity values are associated with carbon. It is known that conductivity of carbon fibers varies over a wide range; and carbon fibers may be manufactured with different dimensions (diameters and lengths). However, reasonable values for σ are on the order of $10^3 - 10^4$ S/m [51]. The other type of inclusions found in the literature is chloroprene rubber inclusions [53], and in this study this material is also considered in Cases 3, 4, and 6 as the host material [51]. Parameters for the other cases in the Table 1 are a combination of those mentioned herein.

The Case 1 is the base case that assumes constant permittivity both for the host and inclusion materials. It is readily suitable for time-domain numerical solution because of the frequency independent values of ε_{eff_D}. Special attention should be paid to Cases 4 and 6 which contain frequency dependencies both for host and inclusion materials. A two-term Debye model should be considered in these cases, as will be detailed below.

2.1. Case 2

Case 2, as from Table 1, is defined as a case, in which the host material has a constant permittivity, and the inclusion material is a Debye-like material.

The expressions for ε_{sD} and $\varepsilon_{\infty D}$ are derived from (4a) and (4b). An equation applicable for both ε_{sD} and $\varepsilon_{\infty D}$,

$$\varepsilon_{LIMx,y,z}(\varepsilon_1, \varepsilon_2) = \frac{\varepsilon_1 (fN_{x,y,z} - N_{x,y,z} - f + 1) + \varepsilon_2 (-fN_{x,y,z} + N_{x,y,z} + f))}{\varepsilon_1 (fN_{x,y,z} - N_{x,y,z} + 1) + \varepsilon_2 (-fN_{x,y,z} + N_{x,y,z})}. \quad (8)$$

is a function of the two generalized parameters ε_1 and ε_2, which should be replaced by the specific material properties ε_e and ε_{is}, respectively,

to calculate $\varepsilon_{sDx,y,z}$, when applying the two limits in (4a) and (4b).

Similarly, $\varepsilon_{\infty Dx,y,z}$ is obtained by substituting $\varepsilon_1 = \varepsilon_e$ and $\varepsilon_2 = \varepsilon_{i\infty}$ to (8). The derived equations for these two parameters can be written as

$$\begin{aligned}\varepsilon_{sDx,y,z} &= \varepsilon_{LIMx,y,z}\left(\varepsilon_e, \varepsilon_{is}\right) \\ &= \frac{\varepsilon_e(\varepsilon_e\left(fN_{x,y,z}-N_{x,y,z}-f+1\right)+\varepsilon_{is}\left(-fN_{x,y,z}+N_{x,y,z}+f\right))}{\varepsilon_e\left(fN_{x,y,z}-N_{x,y,z}+1\right)+\varepsilon_{is}\left(-fN_{x,y,z}+N_{x,y,z}\right)}\end{aligned} \tag{9}$$

$$\begin{aligned}\varepsilon_{\infty Dx,y,z} &= \varepsilon_{LIMx,y,z}\left(\varepsilon_e, \varepsilon_{i\infty}\right) \\ &= \frac{\varepsilon_e(\varepsilon_e\left(fN_{x,y,z}-N_{x,y,z}-f+1\right)+\varepsilon_{i\infty}(-fN_{x,y,z}+N_{x,y,z}+f))}{\varepsilon_e\left(fN_{x,y,z}-N_{x,y,z}+1\right)+\varepsilon_{i\infty}\left(-fN_{x,y,z}+N_{x,y,z}\right)}.\end{aligned} \tag{10}$$

The relaxation time $\tau_{Dx,y,z}$ can be obtained from (7) as

$$\tau_{Dx,y,z} = \frac{\tau_i\left(\varepsilon_e\left(fN_{x,y,z} - N_{x,y,z} + 1\right) + \varepsilon_{i\infty}N_{x,y,z}\left(-f+1\right)\right)}{\varepsilon_e\left(fN_{x,y,z} - N_{x,y,z} + 1\right) + \varepsilon_{is}N_{x,y,z}\left(-f+1\right)}. \tag{11}$$

The three terms in the tensor (1a) are completely defined by the Debye-like permittivity values, as computed by Eqs. (9)–(11) applied to the three directions x, y, and z.

2.2. Case 3

Case 3 is dual to Case 2, and is characterized by a frequency-dependent ε_e and constant ε_i. The parameters $\varepsilon_{sDx,y,z}$ and $\varepsilon_{\infty Dx,y,z}$ in this case are obtained from (8) as

$$\begin{aligned}\varepsilon_{sDx,y,z} &= \varepsilon_{LIMx,y,z}\left(\varepsilon_{es}, \varepsilon_i\right) \\ &= \frac{\varepsilon_{es}\left(\varepsilon_{es}\left(fN_{x,y,z}-N_{x,y,z}-f+1\right)+\varepsilon_i\left(-fN_{x,y,z}+N_{x,y,z}+f\right)\right)}{\varepsilon_{es}\left(fN_{x,y,z}-N_{x,y,z}+1\right)+\varepsilon_i\left(-fN_{x,y,z}+N_{x,y,z}\right)}\end{aligned} \tag{12}$$

$$\begin{aligned}\varepsilon_{\infty Dx,y,z} &= \varepsilon_{LIMx,y,z}\left(\varepsilon_{e\infty}, \varepsilon_i\right) \\ &= \frac{\varepsilon_{e\infty}\left(\varepsilon_{e\infty}\left(fN_{x,y,z}-N_{x,y,z}-f+1\right)+\varepsilon_i\left(-fN_{x,y,z}+N_{x,y,z}+f\right)\right)}{\varepsilon_{e\infty}\left(fN_{x,y,z}-N_{x,y,z}+1\right)+\varepsilon_i\left(-fN_{x,y,z}+N_{x,y,z}\right)}.\end{aligned} \tag{13}$$

The expression for $\tau_{Dx,y,z}$ is given by

$$\begin{aligned}&\tau_{Dx,y,z} = \\ &\frac{\begin{array}{l}-\left(\left(\varepsilon_i-\varepsilon_{es}\right)^2\left(-1+f\right)N_{x,y,z}^2-\left[\left(2-f\right)\varepsilon_{es}+\varepsilon_i f\right]\left(\varepsilon_i-\varepsilon_{es}\right)N_{x,y,z}-\varepsilon_{es}^2\right)\cdot \\ \cdot\tau_e\left[\left(\varepsilon_i-\varepsilon_{e\infty}\right)\left(-1+f\right)N_{x,y,z}-\varepsilon_{e\infty}\right]\end{array}}{\begin{array}{l}-\left(\left(\varepsilon_i-\varepsilon_{es}\right)\left(-1+f\right)N_{x,y,z}-\varepsilon_{es}\right)\cdot \\ \cdot\left(\begin{array}{l}\left(\varepsilon_i-\varepsilon_{e\infty}\right)\left(\varepsilon_i-\varepsilon_{es}\right)\left(f-1\right)N_{x,y,z}^2+ \\ +\left[-\varepsilon_i^2 f+\left(\varepsilon_{es}+\varepsilon_{e\infty}\right)\left(-1+f\right)\varepsilon_i-\varepsilon_{es}\varepsilon_{e\infty}\left(-2+f\right)\right]N_{x,y,z}-\varepsilon_{e\infty}\varepsilon_{es}\end{array}\right)\end{array}}.\end{aligned} \tag{14}$$

2.3. Case 4

This case has both host $\varepsilon_e(\varepsilon_{se},\ \varepsilon_{\infty e},\ \tau_e)$ and inclusions $\varepsilon_i(\varepsilon_{si},\ \varepsilon_{\infty i},\ \tau_i)$ characterized by the Debye dependences. If relaxation times in these two phases are significantly different, real and imaginary parts of the effective permittivity, $\varepsilon_{\mathit{eff}\text{-}MG}$, have, respectively, two pronounced steps and peaks, as in Figures 7. This behavior of $\varepsilon_{\mathit{eff}\text{-}MG}$ looks like the superposition of two Debye terms. To obtain an analytical expression, the host and inclusion Debye dependences should be considered separately, and then simply added together. This approach requires first to approximate the original $\varepsilon_{\mathit{eff}\text{-}MG}$. Three terms are considered

$$\varepsilon_{\mathit{eff}\text{-}MG} \approx \varepsilon_{Part1\text{-}MG} + \varepsilon_{Part2\text{-}MG} - \varepsilon_{Part3\text{-}D}. \tag{15}$$

The first term $\varepsilon_{Part1\text{-}MG}$ is the MGA computed by (1b) with the constant dielectric permittivity $\varepsilon_e = \varepsilon_{e\infty}$ for the host, and the Debye model for the inclusion material $\varepsilon_i(\varepsilon_{si},\ \varepsilon_{\infty i},\ \tau_i)$ is the same as in (3a). The second term $\varepsilon_{Part2\text{-}MG}$ is dual to the first one, so that the host material is the Debye-like $\varepsilon_e(\varepsilon_{se},\ \varepsilon_{\infty e},\ \tau_e)$, and the inclusions have a constant permittivity, $\varepsilon_i = \varepsilon_{i\infty}$. These first two elements describe independently the two Debye dependences. However, the sum of these two terms takes into account twice the values of the high-frequency permittivity for both materials ($\varepsilon_{e\infty}$ and $\varepsilon_{i\infty}$ are included in both $\varepsilon_{Part1\text{-}MG}$ and $\varepsilon_{Part2\text{-}MG}$), introducing a sort of a bias level. To eliminate this bias level, a correction term is introduced, $\varepsilon_{Part3\text{-}D}$. It is constructed directly as a Debye model, whose parameters ($\varepsilon_{s\text{-}Part3}$, $\varepsilon_{\infty\text{-}Part3}$, τ_{Part3}) need to be computed. The three parameters associated with $\varepsilon_{Part3\text{-}D}$ are computed, once $\varepsilon_{Part1\text{-}MG}$ and $\varepsilon_{Part2\text{-}MG}$ are evaluated as in (1b), thus the left side term in (15) and also the first two terms on the right side of (15) can be considered known. The limits of (15) for ω going to zero and infinity are computed. This results in the asymptotic for the static ($\varepsilon_{s\text{-}Part3}$) and high-frequency ($\varepsilon_{\infty\text{-}Part3}$) permittivity of the correction Debye term, respectively.

$$\varepsilon_{s\text{-}Part3} = \lim_{\omega\to 0} \varepsilon_{Part1\text{-}MG} + \lim_{\omega\to 0} \varepsilon_{Part2\text{-}MG} - \lim_{\omega\to 0} \varepsilon_{\mathit{eff}\text{-}MG}. \tag{16a}$$

$$\varepsilon_{s\text{-}Part3} = \lim_{\omega\to \infty} \varepsilon_{Part1\text{-}MG} + \lim_{\omega\to \infty} \varepsilon_{Part2\text{-}MG} - \lim_{\omega\to \infty} \varepsilon_{\mathit{eff}\text{-}MG}. \tag{16b}$$

The τ_{Part3} parameter is found by averaging the relaxation time for the host (τ_e) and inclusion (τ_i) materials,

$$\tau_{Part3} = \frac{\tau_e + \tau_i}{2}. \tag{16c}$$

The set of Eqs. (15), (16) reproduce the MGA model, when both host and inclusions have Debye dependences. The next step is to obtain

an equivalent Debye model from (15). The term $\varepsilon_{Part3\text{-}D}$ is already in a Debye form, thus the conversion from the MGA to the Debye model is required for $\varepsilon_{Part1\text{-}MG}$ and $\varepsilon_{Part2\text{-}MG}$. This procedure is similar to Case 2 for the first term $\varepsilon_{Part1\text{-}MG}$, and to Case 3 for the second term $\varepsilon_{Part2\text{-}MG}$,

$$\varepsilon_{eff\text{-}MG} = \varepsilon_{Part1\text{-}D} + \varepsilon_{Part2\text{-}D} - \varepsilon_{Part3\text{-}D}. \tag{17}$$

2.4. Case 5

Case 5 describes a composite having the constant-permittivity host material, and conductive inclusions, whose complex permittivity is described as in (3b). The parameters of the Debye model analogously to Case 2, and the expression for $\varepsilon_{sDx,y,z}$ can be obtained from (4a) as

$$\varepsilon_{sDx,y,z} = \frac{\varepsilon_e \left(fN_{x,y,z} - N_{x,y,z} - f\right)}{N_{x,y,z}\left(f-1\right)}. \tag{18}$$

The parameter $\varepsilon_{\infty Dx,y,z}$ is evaluated starting from (4b), and resulting in the same form as (8),

$$\begin{aligned}\varepsilon_{\infty Dx,y,z} &= \varepsilon_{LIMx,y,z}\left(\varepsilon_{e\infty}, \varepsilon_{i\infty}\right) \\ &= \frac{\varepsilon_{e\infty}\left(\varepsilon_{e\infty}\left(fN_{x,y,z} - N_{x,y,z} - f + 1\right) + \varepsilon_{i\infty}\left(-fN_{x,y,z} + N_{x,y,z} + f\right)\right)}{\varepsilon_{e\infty}\left(fN_{x,y,z} - N_{x,y,z} + 1\right) + \varepsilon_{i\infty}\left(-fN_{x,y,z} + N_{x,y,z}\right)}.\end{aligned} \tag{19}$$

The relaxation time $\tau_{Dx,y,z}$ can be obtained from (7) as

$$\tau_{Dx,y,z} = \frac{\varepsilon_0\left(\varepsilon_e\left(-fN_{x,y,z} + N_{x,y,z} - 1\right) + \varepsilon_{i\infty}N_{x,y,z}\left(f-1\right)\right)}{\sigma N_{x,y,z}\left(f-1\right)}. \tag{20}$$

2.5. Case 6

In this case, the conductive inclusions with permittivity $\varepsilon_i(\varepsilon_{i\infty},\sigma_i)$, as in (3b), are embedded in a Debye-like host material $\varepsilon_e(\varepsilon_{es},\varepsilon_{e\infty},\tau_e)$, described by (3a). The behavior of the real and imaginary parts of the effective MGA permittivity is very similar to the two-term Debye model, as in Case 4. Therefore, the same three terms in (15) are used to derive the equivalent Debye model that approximates the behavior based on the MGA. The first two terms in (15) are computed based on the procedure analogous to Case 5 (host material with constant $\varepsilon_e = \varepsilon_{e\infty}$ and conductive inclusions, $\varepsilon_i(\varepsilon_{i\infty},\sigma_i)$) for $\varepsilon_{Part1\text{-}MG}$. At the same time, $\varepsilon_{Part2\text{-}MG}$ is evaluated analogously to Case 3 (host material with Debye-like behavior, $\varepsilon_e(\varepsilon_{es},\varepsilon_{e\infty},\tau_e)$, and constant permittivity for the inclusions, $\varepsilon_e = \varepsilon_{i\infty}$). The third term ε_{Part3} in

$$\varepsilon_{eff\text{-}MG} = \varepsilon_{Part1\text{-}MG} + \varepsilon_{Part2\text{-}MG} - \varepsilon_{Part3}, \tag{21}$$

as discussed in [46–49], is set to a constant value. It turns out that the parameters $\varepsilon_{\infty\text{-}Part3}$ and $\varepsilon_{s\text{-}Part3}$, computed as in (16), are so close to each other that their difference is around 1%. Thus, (15) can be further simplified so that Eq. (21) provides a first-order approximation to the MGA, which is later transformed into a sum of Debye terms

$$\varepsilon_{eff\text{-}MG} = \varepsilon_{Part1\text{-}D} + \varepsilon_{Part2\text{-}D} - \varepsilon_{Part3}. \tag{22}$$

The approaches for Case 2 and 3 are applied to the parameters $\varepsilon_{Part1\text{-}MG}$ and $\varepsilon_{Part2\text{-}MG}$, respectively, achieving their Debye counterparts $\varepsilon_{Part1\text{-}D}$ and $\varepsilon_{Part2\text{-}D}$, as given in (22).

3. RESULTS AND DISCUSSION

The equations derived above are applied to the values presented in Table 1 for each case. The real and imaginary parts of the MGA permittivity are evaluated as in (1b) along the three directions x, y, and z, for the tensor (1a). For the sake of brevity only the data associated to the cylindrical inclusions main axes (the z direction) are plotted and compared to the permittivity obtained using the derived equivalent Debye model, for each case. The agreement between the MGA and equivalent Debye is quantified by applying the Feature Selective Validation (FSV) technique [54–57], as required by the IEEE standard P1597. Furthermore, the difference between the effective MG permittivity and the derived equivalent Debye-like dependences are evaluated through the average error (AE)

$$AE = \frac{1}{N} \cdot \sum_{f=1}^{N} \frac{\mathrm{Re}\left(\varepsilon_{eff\text{-}MG}\left(f\right)\right) - \mathrm{Re}\left(\varepsilon_{eq\text{-}Debye}\left(f\right)\right)}{\mathrm{Re}\left(\varepsilon_{eff\text{-}MG}\left(f\right)\right)} \cdot 100. \tag{23}$$

The AE parameter is computed for all the cases under consideration, and only for the largest volume fraction ($f = 20.1\%$). Its value is reported in the figure captions.

In the following examples, the dielectric-dielectric mixtures (Cases 2–4) and the dielectric-conductive (Cases 5, 6) are examined for two different aspect ratio values $a = 5$ and $a = 500$, and for the three different volume fractions of inclusions, $f = 2.5\%$, 8.4%, and 20.1%. As explained before, the volume fraction has, ideally, no limitations due to the percolation effects; however the maximum value considered herein of 20.1% is selected looking at the data and discussions given in [18–25].

3.1. Case 2

In this case, the host material has constant permittivity $\varepsilon_e = 2.2$, and the inclusion permittivity is described with a Debye term ($\varepsilon_{si} = 1900$,

$\varepsilon_{\infty i} = 2804$, and $\tau_i = 2 \cdot 10^{-9}$ s). The parameters (ε_{sD}, $\varepsilon_{\infty D}$, τ_D) of the equivalent Debye model ε_{eff-D} are evaluated by applying the proposed formulation in (9)–(11). The permittivity values are evaluated for different aspect ratios $a = 5$ and 500, and volume fractions of inclusions are set as $f = 2.5\%$, 8.4 %, and 20.1%. The MGA and the Debye results are compared in Figure 2 for the z direction, for aspect ratio $a = 5$. The quantification of the agreement evaluated through the FSV tool is shown in Figure 3 both for the real and imaginary parts of permittivity. There is the perfect agreement between the pair of curves, since the 100% of the Global Difference Measure (GDM) parameter falls within the "Excellent" bar. The same steps are performed for the case with $a = 500$, obtaining the results shown in Figure 4. The FSV agreement evaluation provides exactly the same results as in Figure 4, thus they are omitted for sake of brevity.

In addition to validating the proposed analytical derivation of the Debye model, some observations can be made looking at Figures 2–4, taking into account also the permittivity parameters associated to the x and y directions, evaluated but not shown herein. The high permittivity of the inclusions (much larger than the constant ε_e) affects more the tensor parameter in (1) along the z direction, e.g., for $f = 20.1\%$: $\varepsilon_{sDz} = 11.9$ vs. $\varepsilon_{sDx,y} = 3.37$. Analogous consideration can be made for the imaginary part. It is associated with the dielectric polarization or conductivity losses, which are expected to be higher along the inclusion axes. Furthermore, the inclusions with the higher aspect ratio have larger impact on the equivalent permittivity. The $\varepsilon_{sDz} = 11.9$ for $a = 5$, whereas it is 377, when $a = 500$, allowing much

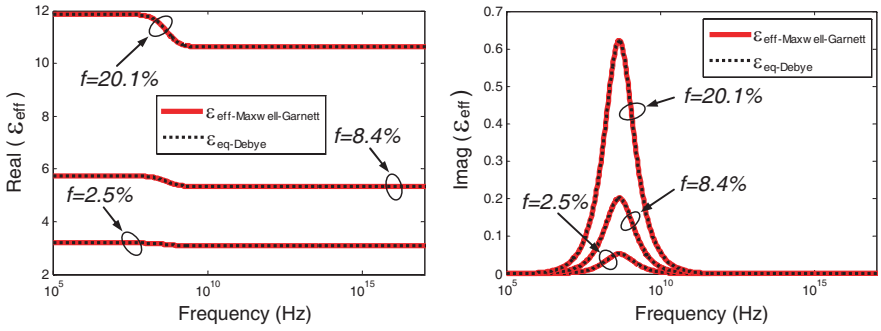

Figure 2. The original MGA model (solid curve) and the computed equivalent Debye model (dashed curve) for Case 2A (z direction) with $a = 5$. (a) Real part. (b) Imaginary part. $AE < 10^{-5}\%$.

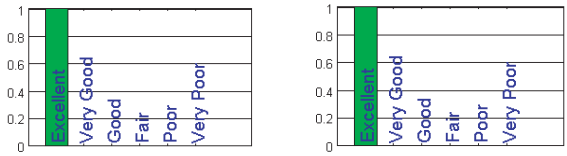

(a) (b)

Figure 3. GDM results for the pair of curve in Figure 2 for $f = 20.1$ and $a = 5$. (a) Real part. (b) Imaginary part.

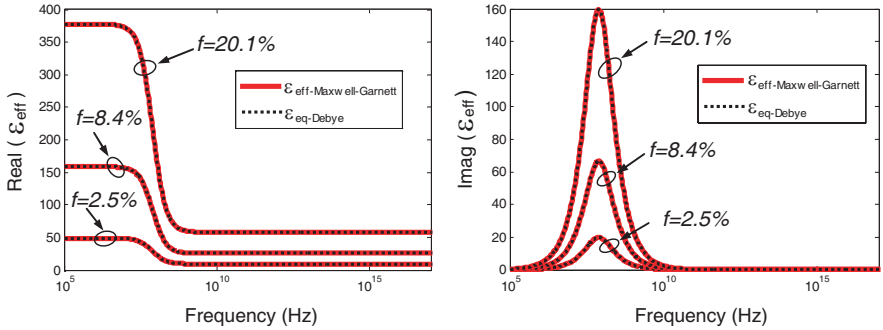

(a) (b)

Figure 4. The original MGA model (solid curve) and the computed equivalent Debye model (dashed curve) for Case 2A (z direction) with $a = 500$. (a) Real part. (b) Imaginary part. $AE < 10^{-5}\%$.

more polarization or conducting effects along the z direction. The aspect ratio a has a negligible effect on the equivalent permittivity along the other directions, x and y, normal to the inclusion axes.

3.2. Case 3

Case 3, according to the input parameters in Table 1, is characterized by inclusions with constant ε_i and the Debye model for ε_e. In the example given herein, chloroprene rubber is considered as a host material (Case 3A, $\varepsilon_{se} = 2.5$, $\varepsilon_{\infty e} = 2.2$, $\tau_e = 8 \cdot 10^{-12}$ s) and inclusions are taken with the constant permittivity ε_i, which corresponds to ε_∞ of the $BaTiO_3$ ($\varepsilon_{\infty i} = 280$). Although both materials are mainly suitable for inclusions, the wide range of their electrical properties is employed herein for the host for a comprehensive validation of this particular Case 3. The same volume fraction values ($f = 2.5$, 8.4 and 20.1%) are used as for the Case 2, varying the aspect ratio, $a = 5$ and $a = 500$ for computing the effective permittivity as in (2) and its equivalent Debye model. The results of the comparison are presented in Figures 5 and 6.

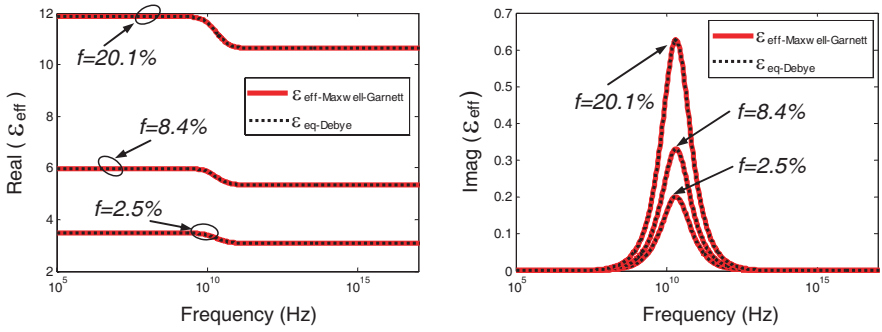

(a) (b)

Figure 5. The original MGA model (solid curve) and the computed equivalent Debye model (dashed curve) for Case 3A (z direction) with $a = 5$. (a) Real part ($AE < 10^{-5}\%$). (b) Imaginary part ($AE = 0.003\%$).

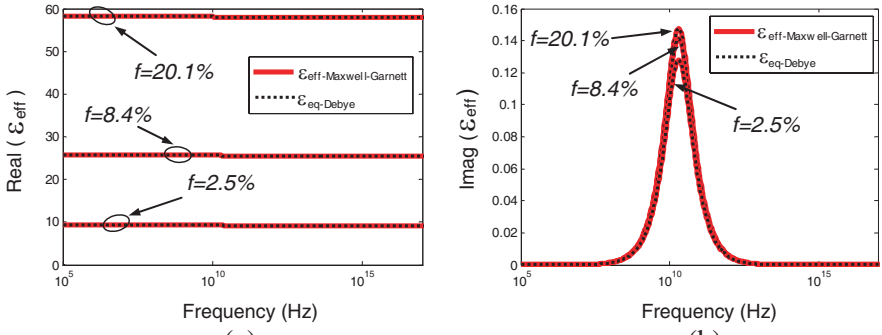

(a) (b)

Figure 6. The original MGA model (solid curve) and the computed equivalent Debye model (dashed curve) for Case 3A (z direction) with $a = 500$. (a) Real part ($AE < 10^{-5}\%$). (b) Imaginary part ($AE = 0.04\%$).

Again, a perfect agreement is found between the original MGA and the derived Debye models. Also, the data processed with the FSV tool, confirm this evaluation (the 100% of the GDM is "Excellent"), thus the FSV results are not shown.

The smaller aspect ratio ($a = 5$) provides an equivalent model with the lower permittivity, as follows from the Figure 5(a), along the z direction. In the case with $a = 500$, the equivalent permittivity is significantly higher, as is seen from Figure 6(a) whereas the values along the x and y directions are basically unaffected by the larger aspect ratio.

3.3. Case 4

This case is related to a composite material with both the host and the inclusion materials characterized by the Debye-like permittivity. In the example Case 4A, the parameters are $\varepsilon_{se} = 2.5$, $\varepsilon_{\infty e} = 2.2$, $\tau_e = 8 \cdot 10^{-12}$ s; $\varepsilon_{si} = 1900$, $\varepsilon_{\infty i} = 280$, $\tau_i = 2 \cdot 10^{-9}$ s. The real and imaginary parts of the resultant permittivity are presented in Figures 7–9. This case, as is mentioned in Section 2 and is seen from Figure 7, has a real part of ε_{eff} with two steps and the imaginary part with a double peak due to the two different material features of host and inclusions. As the aspect ratio increases, the frequency-dependent behavior of the inclusions becomes dominating. Thus, the results for the Case 4A with $a = 500$ provide just one step in the real part of ε_{eff} and one peak in the imaginary part of ε_{eff}, as Figure 9 shows. Although in this case the agreement is not perfect, the proposed formulation provides an equivalent Debye model very close to the original MGA

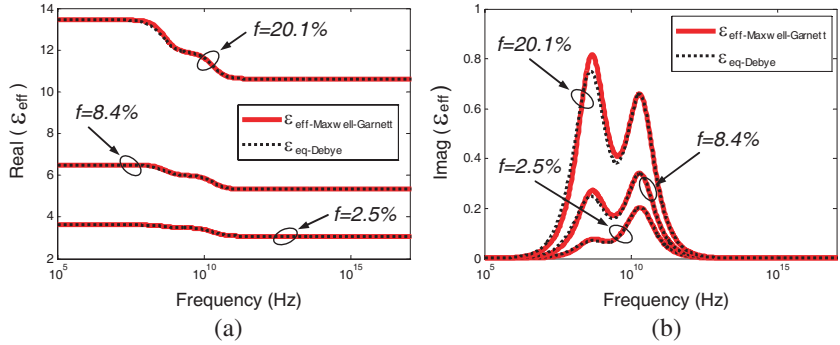

Figure 7. The original MGA model (solid curve) and the computed equivalent Debye model (dashed curve) for Case 4A (z direction) with $a = 5$. (a) Real part ($AE = 0.05\%$). (b) Imaginary part ($AE = 14\%$).

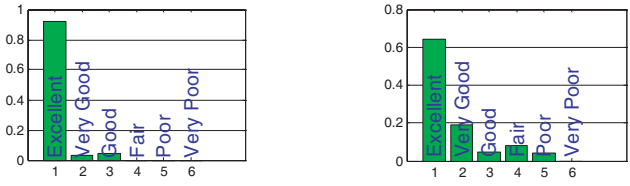

Figure 8. The original MGA model (solid curve) and the computed equivalent Debye model (dashed curve) for Case 4A (z direction) with $a = 500$. (a) Real part ($AE = 0.014\%$). (b) Imaginary part ($AE = 0.1\%$).

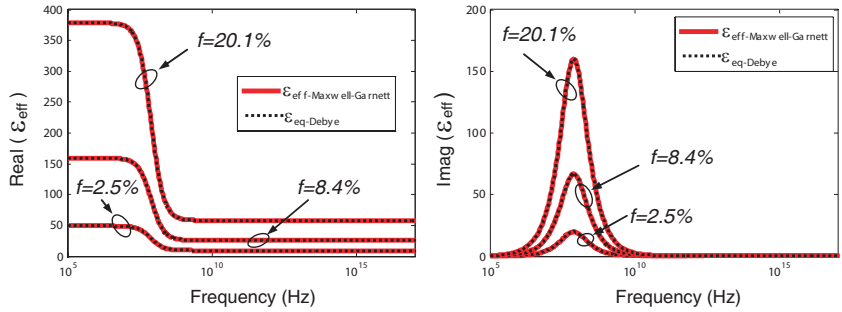

(a) (b)

Figure 9. The original MGA model (solid curve) and the computed equivalent Debye model (dashed curve) for Case 4A (z direction) with $a = 500$. (a) Real part ($AE = 0.014\%$). (b) Imaginary part ($AE = 0.1\%$).

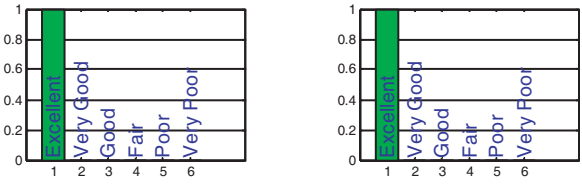

(a) (b)

Figure 10. GDM results for the pair of curve in Figure 14 for $f = 20.1$ and $a = 500$. (a) Real part. (b) Imaginary part.

effective permittivity. The FSV results help quantifying the difference, and it is run for the two considered cases (Case 4A with $a = 5$ and 500), only for the principal direction (z). The worst results are those in Figure 7, but the quantification of the agreement through the FSV tool given in Figure 8 still provides a positive judgement, since the "Excellent" bar is still the prevalent one. The FSV tool quantifies with a full "Excellent" bar, as in Figure 10, the perfect agreement of the data in Figure 9.

3.4. Case 5

The Case 5 is associated with conductive inclusions ε_i. In the example Case 5A, $\varepsilon_{i\infty} = 2$, $\sigma_i = 4 \cdot 10^3$, and in Case 5B, $\sigma_i = 4 \cdot 10^4$ embedded in a constant $\varepsilon_e = 2.2$. The results in Figures 11 and 12 show perfect agreement between the two models, independently upon the volume fraction f, aspect ratio a, and inclusion conductivity. The FSV results provide a 100% "Excellent" parameter, thus the detailed figures are omitted.

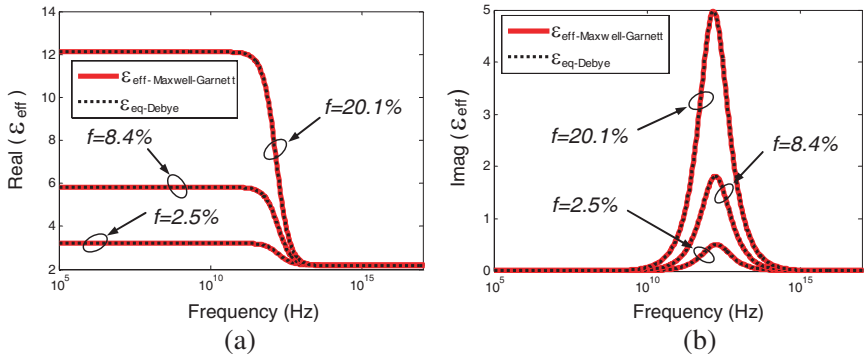

Figure 11. The original MGA model (solid curve) and the computed equivalent Debye model (dashed curve) for Case 5A (z direction) with $a = 5$. (a) Real part ($AE < 10^{-5}\%$). (b) Imaginary part ($AE < 10^{-5}\%$).

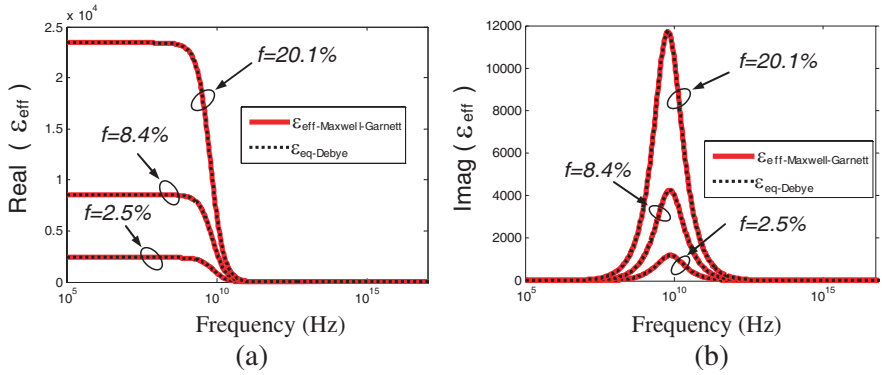

Figure 12. The original MGA model (solid curve) and the computed equivalent Debye model (dashed curve) for Case 5B (z direction) with $a = 500$. (a) Real part ($AE < 10^{-5}\%$). (b) Imaginary part ($AE < 10^{-5}\%$).

3.5. Case 6

The Case 6 is related to conductive inclusions embedded in a host material with the Debye behavior. The results are presented in Figures 13–15. Although all computations are performed for the three volume fraction $f = 2.5\%$, 8.4%, and 20.1%, the FSV tool is applied to the cases with $f = 20.1\%$, providing the results in Figure 14 and Figure 16. As is seen from the Figure 13 compared to Figure 15, the larger aspect ratio ($a = 500$ vs. $a = 5$) makes the model more

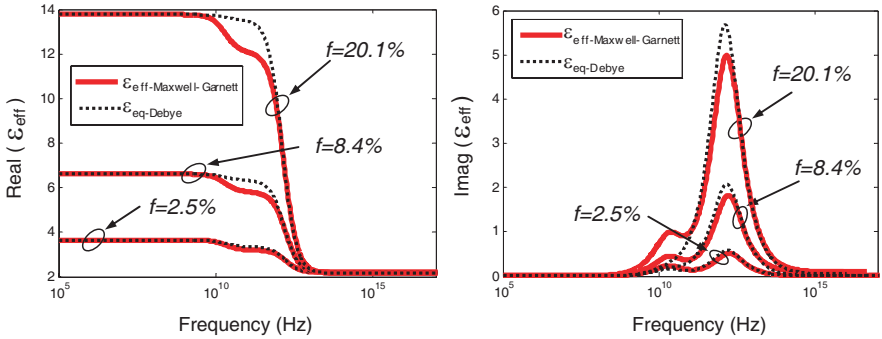

Figure 13. The original MGA model (solid curve) and the computed equivalent Debye model (dashed curve) for Case 6A (z direction) with $a = 5$. (a) Real part ($AE = 0.8\%$). (b) Imaginary part ($AE = 39.8\%$).

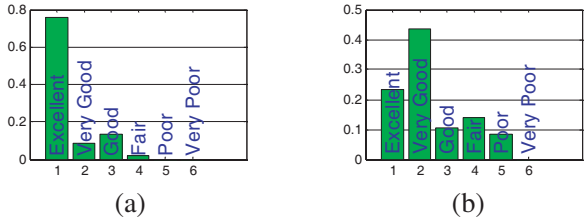

Figure 14. GDM results for the pair of curve in Figure 13 for $f = 20.1\%$ and $a = 5$. (a) Real part. (b) Imaginary part.

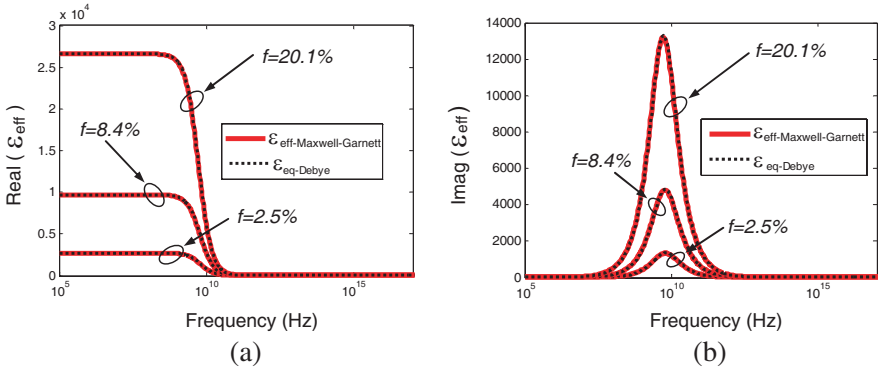

Figure 15. The original MGA model (solid curve) and the computed equivalent Debye model (dashed curve) for Case 6B (z direction) with $a = 500$. (a) Real part ($AE = 0.6\%$). (b) Imaginary part ($AE = 1.3\%$).

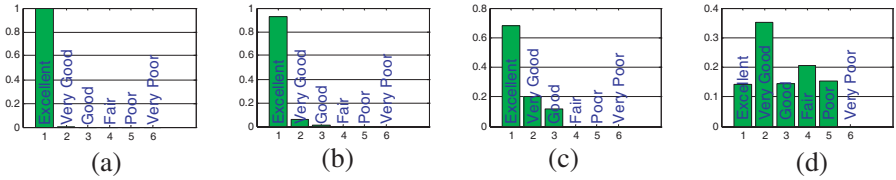

Figure 16. GDM results for the pair of curve in Figure 15 for $f = 20.1$ and $a = 500$. (a) Real part. (b) Imaginary part; and for $f = 20.1$ and $a = 500$. (c) Real part. (d) Imaginary part.

accurate. This is related to the dominant behavior of the conducting inclusions in forming the Debye peak over the host. It is possible to state this conclusion also by looking at the FSV results in Figure 14 and Figure 16.

4. SIMULATION EXAMPLE

The validation of the derived equations that correlate the MGA and its rational-fractional representation through the Debye model can be illustrated by a numerical simulation example. For this purpose, the same composite as in Case 2 is considered. It contains aligned inclusions of $BaTiO_3$ with the intrinsic dispersive Debye parameters $\varepsilon_{is} = 1900$, $\varepsilon_{i\infty} = 280$, and $\tau_i = 2 \cdot 10^{-9}$ s placed in a host material with constant permittivity $\varepsilon_e = 2.2$. The aspect ratio of inclusions is $a = 500$, and the inclusion volume fractions are $f = 2.5$, 8.4 and 20.1%. The real and imaginary parts the effective dielectric permittivity of the original MG model (1b) and the computed equivalent Debye model (8)–(10) are shown in Figure 4, respectively.

Then two models for 3D numerical simulations are created. Model 1 contains cylindrical inclusions, and Model 2 contains the homogeneous material with the equivalent Debye parameters. In Model 1, the inclusion radius is r, length is l, and the panel thickness is W. These parameters are related as

$$f = \frac{\text{Inclusion Volume}}{\text{Total Volume}} = \frac{\pi \cdot r^2 \cdot l}{W^2 \cdot l} = \frac{\pi \cdot r^2}{W^2}. \tag{24}$$

$$a = \frac{\text{Inclusion Length}}{\text{Inclusion Diameter}} = \frac{l}{d} = \frac{l}{2 \cdot r} \tag{25}$$

One parameter can be fixed, e.g., r is chosen 0.1 mm, and the other two, W and l, are calculated. This is done for each abovementioned volume fraction values. Table 2 contains the complete set of the geometrical and calculated equivalent Debye parameters along all three

directions. The parameters of the Debye model are associated to the curves in Figure 4.

The simulations are done using the time domain solver within CST Microwave Studio [58], on a workstation with an Intel Xeon CPU E5520 at 2.27 GHz, with 24 GB of RAM. In these simulations, the modeled structure is excited by a plane wave source 1 mm before the composite panel (at $x = -1$ mm), and the E-field is evaluated 25 mm behind the composite layer (at $x = W + 25$ mm). The periodic boundary conditions are applied along the y and $z$directions to provide an infinite structure along these directions. It is important to note that, in the simulation model, just one block is simulated, as shown in Figure 17. The host material covers entirely the inclusions along the z direction for avoiding adjacent inclusions to touch each other (as emulated by the periodic boundary conditions applied along the z direction); thus an extra length to the host material is added $s = r/2$ (0.5 mm). The term l in the denominator of (24) should be replaced by $(l + 2s)$. However, since $l \gg s$ in the case of $a = 500$, then s is neglected in (24).

The simulation settings of the six 3D models are summarized in

Table 2. Parameters overview of the three simulation models.

a	r (mm)	f	l (mm)	W (mm)	$\varepsilon_{sDx}=\varepsilon_{sDy}$	$\varepsilon_{\infty Dx}=\varepsilon_{\infty Dy}$	$\tau_{Dx}=\tau_{Dy}$ (s)	ε_{sDz}	$\varepsilon_{\infty Dz}$	τ_{Dz} (s)
500	0.1	2.5	100	1.12	2.3125	2.3110	$3.057\cdot10^{-10}$	48.720	9.124	$2.0257\cdot10^{-9}$
500	0.1	8.4	100	0.6115	2.6024	2.5966	$3.0598\cdot10^{-10}$	158.693	25.4715	$2.0277\cdot10^{-9}$
500	0.1	20.1	100	0.395	3.3037	3.2854	$3.0663\cdot10^{-10}$	377.544	57.9050	$2.0318\cdot10^{-9}$

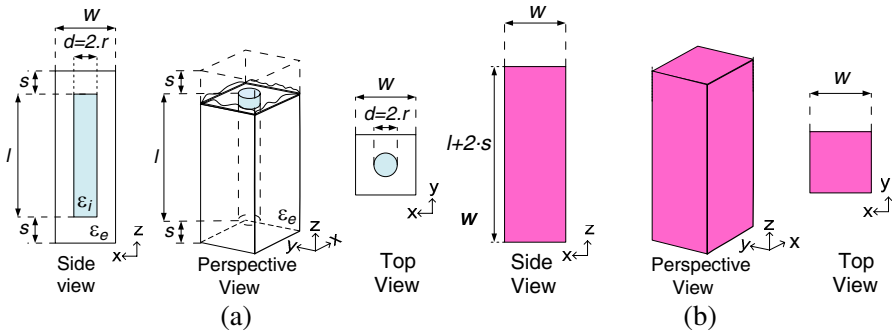

Figure 17. (a) The proposed geometries containing cylindrical inclusions, model 1. (b) Its equivalent homogeneous models, model 2.

Table 3. Simulation parameters.

f	*Models*	*Run time*	*Mesh cells*	*Mesh cells on cross-section*
2.5	Model-1	67 min 36 sec	1291864	31×31
	Model-2	4 sec	105000	7×7
8.4	Model-1	96 min 35 sec	1882440	30×30
	Model-2	11 sec	208208	7×7
20.1	Model-1	166 min 42 sec	3706238	34×34
	Model-2	25 sec	359310	7×7

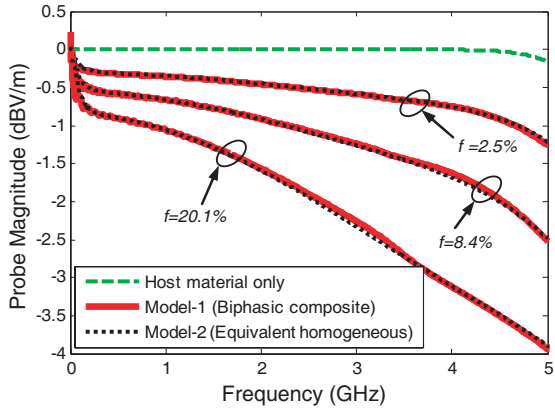

Figure 18. Probe magnitude simulation result comparison.

Table 3. The simulated results in terms of the *E*-field transmitted through the simulation sample, are compared in Figure 18 in the frequency range up to 5 GHz.

The simulation results show that the agreement between Models 1 and 2 is excellent for all three inclusion volume fractions. The FSV tool is employed to quantify the data agreement. The GDM results are shown in Figure 19. It is important to note that the simulation of the homogenous Model 2 is almost 200 times faster than the simulation of the biphasic Model 1. These results, beside confirming the correctness of the Maxwell Garnett approximation up to the 20.1% volume fraction considered in our validation cases for a dielectric-dielectric mixture, prove the usefulness of the derived analytical equivalence between the

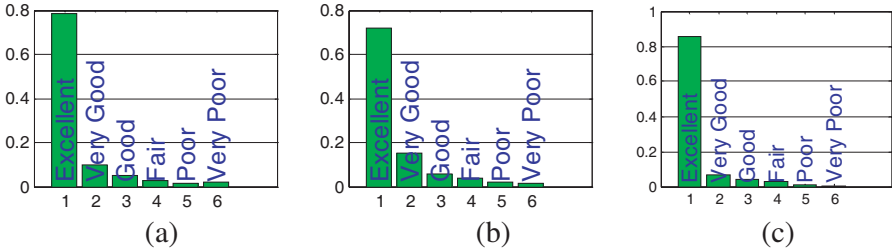

Figure 19. GDM results for the pair of curve in Figure 18 for (a) $f = 2.5\%$ (Grade = 2, Spread = 2), (b) $f = 8.4\%$ (Grade = 2, Spread = 2), (c) $f = 20.1\%$ (Grade = 1, Spread = 1).

Maxwell Garnett and the Debye model. The equivalent homogeneous model, initially obtained applying the MGA to the biphasic composite, and then converted into a Debye model, allows a quick and efficient simulation of the electromagnetic behavior of the original biphasic composite material.

5. CONCLUSION

The composite materials containing aligned cylindrical inclusions embedded in a host material are studied by using the geometry-based Maxwell Garnett approximation (MGA). The equivalent Debye model is derived from some analytical relations between the two models. The analytical derivations are obtained for the typical combinations of permittivity types of host and inclusion materials, i.e., material with constant permittivity, dispersive (described by a Debye model), and conductive materials, and analytical expressions are derived for each case. The validation for the five types of material combinations is done numerically. The dielectric and conductivity parameters of some commercial shielding materials are used in these computations. The best agreement between the MGA and its derived equivalent Debye model is obtained, when only one ingredient in a biphasic mixture has a frequency dispersive behavior, while the other is non-dispersive. However, the agreement is still acceptable in the cases, when both phases are the Debye materials, or the host is the Debye material, while inclusion phase is conductive (Cases 4 and 6). The proposed approach can be used to analytically obtain the Debye parameters starting from the MGA, without the need of curve-fitting and applying optimization techniques. Thus a causal model for complex dielectrics suitable for time domain electromagnetic simulations can be readily built.

ACKNOWLEDGMENT

The co-authors from Missouri University of Science & Technology acknowledge partial support of this study by a National Science Foundation (NSF) grant (#0855878) through the I/UCRC program.

APPENDIX A.

Herein the proof that the Debye model satisfies the Kramer-Kronig relationship is derived, based on the theory in [59, 60]. A general first order Debye model can be written as in (A1), similarly to (3a). The real part and imaginary parts computed starting from (A1) are given in (A2).

$$\varepsilon_D(\omega) = \varepsilon_\infty + \frac{(\varepsilon_s - \varepsilon_\infty)}{1 + j\omega\tau}, \tag{A1}$$

$$\varepsilon_R(\omega) = \mathrm{Re}\left[\varepsilon_D(\omega)\right] = \varepsilon_\infty + \frac{(\varepsilon_s - \varepsilon_\infty)}{1 + \omega^2\tau^2}, \tag{A2a}$$

$$\varepsilon_I(\omega) = \mathrm{Im}\left[\varepsilon_D(\omega)\right] = -\omega\tau\frac{(\varepsilon_s - \varepsilon_\infty)}{1 + \omega^2\tau^2}. \tag{A2b}$$

The KKR associated to the complex frequency dependent parameter $\varepsilon_D(\omega)$ are given in (A3), considering the derivation of the imaginary part starting from the real part and viceversa,

$$\varepsilon_I(\omega') = -\frac{1}{\pi}P\int_{-\infty}^{\infty}\frac{\varepsilon_R(\omega)}{\omega - \omega'}d\omega, \tag{A3a}$$

$$\varepsilon_R(\omega') = \frac{1}{\pi}P\int_{-\infty}^{\infty}\frac{\varepsilon_I(\omega)}{\omega - \omega'}d\omega, \tag{A3b}$$

where P refers to the Cauchy principal value since the integrand function is singular in $\omega = \omega'$. The analytical derivation is applied next to the case in (A3a). The integral can be solved applying the residue theorem, considering a complex domain for ω, as from Figure A1. The integral should be computed along the closed contour C taken counterclockwise made by the partial paths C_R, P, and γ, thus bypassing the singularity on the contour at $\omega = \omega'$. Since the function $\varepsilon_R(\omega)$ has a pole at $\omega = j/\tau$, the integral along the close contour is equal to the residue computed at this pole, as from (A4).

$$\oint_C f(\omega)\,d\omega = \int_{C_R} f(\omega)\,d\omega + \int_P f(\omega)\,d\omega + \int_\gamma f(\omega)\,d\omega = 2\pi j \cdot \mathrm{Res}\left[f(j/\tau)\right], \tag{A4}$$

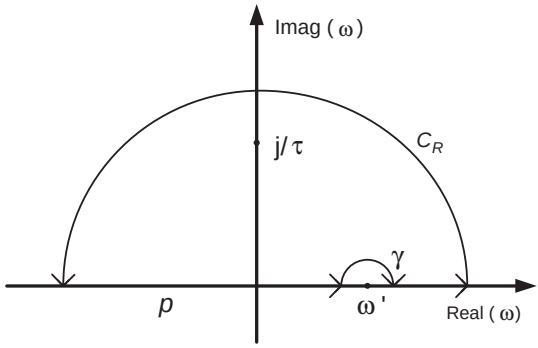

Figure A1. Complex domain and integration path for evaluating the Cauchy principal value.

where $f(\omega)$ is the overall integrand function in (A3a).

The first integral along C_R can be evaluated as in (A5), making the variable substitution $z = R \cdot e^{j\theta}$, thus $dz = jR \cdot e^{j\theta} d\theta$.

$$\int_{C_R} f(z)\, dz = \lim_{R\to\infty} \int_0^{\pi} f\left(R \cdot e^{j\vartheta}\right) jR \cdot e^{j\vartheta} d\vartheta = j\pi\varepsilon_\infty, \tag{A5}$$

The integral over the semicircle γ is calculated as in (A6) by noting that $z = \omega' - \varepsilon \cdot e^{j\theta}$ and $dz = j\varepsilon \cdot e^{j\theta} d\theta$.

$$\int_{\gamma} f(z)\, dz = \int_{\pi}^{0} f\left(\omega' + \varepsilon e^{j\vartheta}\right) j\varepsilon e^{j\vartheta} d\vartheta = -j\pi \frac{\varepsilon_s + \varepsilon_\infty \omega'^2 \tau^2}{1 + \omega'^2 \tau^2}, \tag{A6}$$

The residue in (A4) follows the calculation in (A7)

$$\mathrm{Res}\left[f(j/\tau)\right] = \lim_{z\to j/\tau} f(z)(z - j/\tau) = \frac{\varepsilon_s - \varepsilon_\infty}{2j(j - \omega'\tau)}, \tag{A7}$$

Thus the principal value of the integral in (A3) can be finally evaluated obtaining the result in (A8).

$$P \int_{-\infty}^{\infty} \frac{\varepsilon_R(\omega)}{\omega - \omega'} d\omega = \omega'\tau\pi \frac{\varepsilon_\infty - \varepsilon_s}{1 + \omega'^2\tau^2}, \tag{A8}$$

After multiplying the result in (A8) by $-1/\pi$ from (A3a), the expression in (A2b) is obtained, demonstrating analytically that the frequency dependent dielectric permittivity described by a Debye model satisfies the KKR, thus it is causal by definition. Similarly the dual procedure can be applied to (A3b).

REFERENCES

1. Chou, T.-C., M.-H. Tsai, and C.-Y. Chen, "A low insertion loss and high selectivity UWB bandpass filter using composite right/left-handed material," *Progress In Electromagnetics Research C*, Vol. 17, 163–172, 2010.
2. Galehdar, A., W. S. T. Rowe, K. Ghorbani, P. J. Callus, S. John, and C. H. Wang, "The effect of ply orientation on the performance of antennas in or on carbon fiber composites," *Progress In Electromagnetics Research*, Vol. 116, 123–136, 2011.
3. De Rosa, I. M., R. Mancinelli, F. Sarasini, M. S. Sarto, and A. Tamburrano, "Electromagnetic design and realization of innovative fiber-reinforced broad-band absorbing screens," *IEEE Transactions on Electromagnetic Compatibility*, Vol. 51, No. 3, 700–707, August 2009.
4. Koledintseva, M. Y., R. E. DuBroff, and R. W. Schwartz, "A Maxwell Garnett model for dielectric mixtures containing conducting particles at optical frequencies," *Progress In Electromagnetics Research*, Vol. 63, 223–242, 2006.
5. Koledintseva, M. Y., S. K. R. Chandra, R. E. DuBroff, and R. W. Schwartz, "Modeling of dielectric mixtures containing conducting inclusions with statistically distributed aspect ratio," *Progress In Electromagnetics Research*, Vol. 66, 213–228, 2006.
6. Jylha, L. and A. H. Sihvola, "Tunability of granular ferroelectric dielectric composites," *Progress In Electromagnetics Research*, Vol. 78, 189–207, 2008.
7. Teirikangas, M., J. Juuti, and H. Jantunen, "Organic-inorganic RF composites with enhanced permittivity by nanoparticle additions," *Progress In Electromagnetics Research*, Vol. 115, 147–157, 2011.
8. Liao, Y., C. Zhang, Y. Zhang, V. Strong, J. Tang, X. Li, K. Kalantar-zadeh, E. M. V. Hoek, K. L. Wang, and R. B. Kaner, "Carbon nanotube/polyaniline composite nanofibers: Facile synthesis and chemosensors," *Nano Letters*, Vol. 11, 954–959, 2011.
9. Santos, J., B. Lopes, and P. J. Costa Branco, "Ionic polymer-metal composite material as a diaphragm for micropump devices," *Sensors and Actuators A: Physical*, Vol. 161, 225–233, June 2010.
10. Wang, J., J. Chen, K. Konstantinov, L. Zhao, S. H. Ng, G. X. Wang, Z. P. Guo, and H. K. Liu, "Sulphur-polypyrrole composite positive electrode materials for rechargeable lithium batteries," *Electrochimica Acta*, Vol. 51, 4634–4638, June 2006.

11. Winther-Jensen, B., K. Fraser, C. Ong, M. Forsyth, and D. R. MacFarlane, "Conducting polymer composite materials for hydrogen generation," *Advanced Materials*, Vol. 22, No. 15, 1727–1730, April 2010.
12. Gao, D. and L. Gao, "Tunable lateral shift through nonlinear composites of nonspherical particles," *Progress In Electromagnetics Research*, Vol. 99, 273–287, 2009.
13. Bruggeman, D. A. G., "Berechnung verschiedener physikalischer konstanten von heterogenen substanzen," *Annalen der Physik*, Vol. 5, No. 24, 636–679, 1936.
14. McLachlan, D. S., A. Priou, I. Chernie, E. Isaac, and E. Henry, "Modeling the permittivity of composite materials with general effective medium equation," *Journal of Electromagnetic Waves and Applications*, Vol. 6, No. 6, 1099–1131, 1992.
15. Maxwell Garnett, J. C., "Colours in metal glasses and metal films," *Philos. Trans. R. Soc. London, Sect. A*, Vol. 3, 385–420, 1904.
16. Tinga, W. R., W. A. G. Voss, and D. F. Blossey, "Generalized approach to multiphase dielectric mixture theory," *J. Appl. Phys.*, Vol. 44, No. 9, 3897–3902, 1973.
17. Levy, O. and D. Stroud, "Maxwell Garnett theory for mixtures of anisotropic inclusions: Application to conducting polymers," *Phys. Rev. B*, Vol. 56, No. 13, 8035–8046, October 1997.
18. Moiseev, S. G., "Active Maxwell-Garnett composite with the unit refractive index," *Physica B: Condensed Matter*, Vol. 405, No. 14, 3042–3045, 2010.
19. Lagarkov, A. N. and A. K. Sarychev., "Electromagnetic properties of composites containing elongated conducting inclusions," *Physical Review B*, Vol. 53, 6318–6336, March 1996.
20. Ruppin, R., "Evaluation of extended Maxwell-Garnett theories," *Optics Communications*, Vol. 182, 273–279, August 2000.
21. Lu, S. Y. and H. C. Lin, "Effective conductivity of composites containing aligned spheroidal inclusions of finite conductivity," *J. Appl. Phys.*, Vol. 79, 6761–6769, 1996.
22. Skryabin, I. L., A. V. Radchik, P. Moses, and G. B. Smith, "The consistent application of Maxwell-Garnett effective medium theory to anisotropic composites," *Appl. Phys. Lett.*, Vol. 70, 2221–2223, April 1997.
23. Sihvola, A. H., "Self-consistency aspects of dielectric mixing theories," *IEEE Trans. on Geoscience and Remote Sensing*, Vol. 27, 403–415, July 1989.

24. Garcia-Vidal, F. J., J. M. Pitarke, and J. B. Pendry, "Effective medium theory of the optical properties of aligned carbon nanotubes," *Phys. Rev. Lett.*, Vol. 78, 4289–4292, 1997.
25. Ao, C. O., "Electromagnetic wave scattering by discrete random media with remote sensing applications," Ph.D. dissertation, Dept. Physics, Massachusetts Institute of Technology, Cambridge, MA, June 2001.
26. Brosseau, C., A. Beroual, and A. Boudida, "How shape anisotropy and spatial orientation of the constituents affect the permittivity of dielectric hetero structures?" *J. Appl. Phys.*, Vol. 88, 7278–7288, 2000.
27. Ao, C. O. and J. A. Kong, "Analytical approximations in multiple scattering of electromagnetic waves by aligned dielectric spheroids," *J. Opt. Soc. Am. A*, Vol. 19, 1145–1156, June 2002.
28. Barrera, R. G., J. Giraldo, and W. L. Mochan, "Effective dielectric response of a composite with aligned spheroidal inclusions," *Phys. Rev. B*, Vol. 47, No. 4, 8528–8538, April 1993.
29. Varadan, V. V. and V. K. Varadan, "Anisotropic dielectric properties of media containing aligned non-spherical scatterers," *IEEE Trans. Antennas and Propagation*, Vol. 33, No. 8, 886–890, August 1985.
30. Xu, X., A. Qing, Y. B. Gan, and Y. P. Feng, "Effective properties of fiber composite materials," *Journal of Electromagnetic Waves and Applications*, Vol. 18, No. 5, 649–662, 2004.
31. Srivastava, V. K., U. Gabbert, H. Berger, and S. Singh, "Analysis of particles loaded fiber composites for the evaluation of effective material properties with the variation of shape and size," *International Journal of Engineering, Science and Technology*, Vol. 3, No. 1, 52–68, 2011.
32. Antonini, G., A. Orlandi, and V. Ricchiuti, "Causality check for si data validation," *9th IEEE Workshop on Signal Propagation on Interconnects*, Garmish-Partenkirchen, Ge, May 2005.
33. Mandrekar, R. and M. Swaminathan, "Delay extraction from frequency domain data for causal macro-modeling of passive networks," *IEEE International Symposium on Circuits and Systems*, Vol. 6, 5758–5761, May 2005.
34. Triverio, P. and S. G. Talocia, "A robust causality verification tool for tabulated frequency data," *10th IEEE Workshop on Signal Propagation on Interconnects*, Berlin, Ge, May 2006.
35. Koledintseva, M. Y., J. Wu, J. Zhang, J. L. Drewniak, and K. N. Rozanov, "Representation of permittivity for multi-

phase dielectric mixtures in FDTD modeling," *Proc. IEEE Symp. Electromag. Compat.*, Santa Clara, CA, Vol. 1, 309–314, August 2004.

36. Nisanci, M. H., F. De Paulis, M. Y. Koledintseva, and A. Orlandi, "Use of Maxwell Garnett model for random and aligned cylindrical inclusions in full wave EMC simulations," *IEEE International Symposium on Electromagnetic Compatibility*, Long Beach, CA, August 2011.
37. Koledintseva, M. Y., R. E. DuBroff, and R. W. Schwartz, "Maxwell Garnett rule for dielectric mixtures with statistically distributed orientations of inclusions," *Progress In Electromagnetics Research*, Vol. 99, 131–148, 2009.
38. Sihlova, A. H. and J. A. Kong, "Effective permittivity of dielectric mixtures," *IEEE Trans. on Geoscience and Remote Sensing*, Vol. 26, 420–429, July 1988.
39. Koledintseva, M. Y., R. E. DuBroff, R. W. Schwartz, and J. L. Drewniak, "Double statistical distribution of conductivity and aspect ratio of inclusions in dielectric mixtures at microwave frequencies," *Progress In Electromagnetics Research*, Vol. 77, 193–214, 2007.
40. Sihvola, A., "Electromagnetic mixing formulas and applications," *IEE*, London, UK, 1999.
41. Landau, L. D., E. M. Lifshitz, and L. P. Pitaevskii, *Electrodynamics of Continuous Media*, 2nd revised edition, Oxford, Pergamon, 1984.
42. Park, H. S., I. S. Choi, J. K. Bang, S. H. Suk, S. S. Lee, and H. T. Kim, "Optimized design of radar absorbing materials for complex targets," *Journal of Electromagnetic Waves and Applications*, Vol. 18, No. 8, 1105–1117, 2004.
43. Meng, Z. Q., "Autonomous genetic algorithm for functional optimization," *Progress In Electromagnetics Research*, Vol. 72, 253–268, 2007.
44. Donelli, M., S. Caorsi, F. de Natale, D. Franceschini, and A. Massa, "A versatile enhanced genetic algorithm for planar array design," *Journal of Electromagnetic Waves and Applications*, Vol. 18, No. 11, 1533–1548, 2004.
45. Koledintseva, M., K. Rozanov, and J. Drewniak, "Engineering, modeling and testing of composite absorbing materials for EMC applications," *Advances in Composite Materials — Ecodesign and Analysis*, Chapter 13, 291–316, Brahim Attaf, InTech, March 2011.

46. De Paulis, F., M. H. Nisanci, M. Y. Koledintseva, and A. Orlandi, "From Maxwell Garnett to Debye model for electromagnetic simulation of composite dielectrics. Part I: Random spherical inclusions," *IEEE Trans. Electromag. Compat.*, 2011.
47. http://orlandi.ing.univaq.it/Uaq_Laboratory/docs/mg2d/Equations_Part_I.pdf.
48. Nisanci, M. H., F. De Paulis, M. Y. Koledintseva, and A. Orlandi, "From Maxwell Garnett to Debye model for electromagnetic simulation of composite dielectrics. Part II: Random cylindrical inclusions," *IEEE Trans. Electromag. Compat.*, 2011.
49. http://orlandi.ing.univaq.it/Uaq_Laboratory/docs/mg2d/Equations_Part_II.pdf.
50. Teflon Dielectric Properties, http://www.dupont.com/Teflon_Industrial/en_US/products/product_by_name/teflon, November 2010.
51. Koledintseva, M. Y., J. Drewniak, and R. DuBroff, "Modeling of shielding composite materials and structures for microwave frequencies," *Progress In Electromagnetics Research B*, Vol. 15, 197–215, 2009.
52. Cho, K. H. and H. Y. Lee, "Pore-dependent dielectric and electrical properties of barium titanate ceramic," *Proceedings of the Ninth IEEE International Symposium on Applications of Ferroelectrics*, University Park, PA, USA., August 1991.
53. Norman, R. H., *Electrically Conducting Rubber Composites*, Elsevier, Oxford, 1970.
54. IEEE Standard P1597, *Standard for Validation of Computational Electromagnetics Computer Modeling and Simulation*, Part 1, 2, 2008.
55. Duffy, A. P., A. J. M. Martin, A. Orlandi, G. Antonini, T. M. Benson, and M. S. Woolfson, "Feature selective validation (FSV) for validation of computational electromagnetics (CEM). Part I — The FSV method," *IEEE Trans. on Electromagn. Compatibility*, Vol. 48, No. 3, 449–459, 2006.
56. Orlandi, A., A. P. Duffy, B. Archambeault, G. Antonini, D. E. Coleby, and S. Connor, "Feature selective validation (FSV) for validation of computational electromagnetics (CEM). Part II — Assessment of FSV performance," *IEEE Trans. on Electromagn. Compatibility*, Vol. 48, No. 3, 460–467, 2006.
57. Orlandi, A., FSV Tool, 2011, downloadable at http://uaqemc.ing.univaq.it/uaqemc/FSV_Tool_2_0_0L/.

58. Computer Simulation Technology, *CST Studio Suite*, 2011, [Online], Available: http://www.cst.com/.
59. Oppenheim, A. V., R. W. Schafer, and J. R. Buck, *Discrete-time Signal Processing*, Ch. 2, 8, 10, and 11, 2nd edition, Prentice Hall Inc., 1999.
60. Hahn, S. L., *Hilbert Transform in Signal Processing*, Artech House Publishers, 2000.